Available online at www.sciencedirect.com

ScienceDirect

Procedia IUTAM 10 (2014) 396 – 409

Procedia IUTAM

www.elsevier.com/locate/procedia

23rd International Congress of Theoretical and Applied Mechanics

# Modelling the evolution of cerebral aneurysms: Biomechanics, mechanobiology and multiscale modelling

Alisa Selimovic, Yiannis Ventikos, Paul N. Watton*

*Department of Engineering Science, University of Oxford, Oxford OX1 3PJ, UK*

**Abstract**

Intracranial aneurysms (IAs) are abnormal dilatations of the cerebral vasculature. Computational modelling may shed light on the aetiology of the disease and lead to improved criteria to assist diagnostic decisions. We briefly review models of aneurysm evolution to date and present a novel fluid-solid-growth (FSG) framework for patient-specific modelling of IA evolution. We illustrate its application to 4 clinical cases depicting an IA. The section of arterial geometry containing the IA is removed and replaced with a cylindrical section: this represents an idealised section of healthy artery upon which IA evolution is simulated. The utilisation of patient-specific geometries enables G&R to be explicitly linked to physiologically realistic spatial distributions and magnitudes of haemodynamic stimuli. In this study, we investigate the hypothesis that elastin degradation is driven by locally low wall shear stress (WSS). In 3 out of 4 cases, the evolved model IA geometry is qualitatively similar to the corresponding in vivo IA geometry. This suggests some tentative support for the hypothesis that low WSS plays a role in the mechanobiology of IA evolution.


Selection and/or peer-review under responsibility of the Organizing Committee of The 23rd International Congress of Theoretical and Applied Mechanics, ICTAM2012

*Keywords*: intracranial aneurysm, evolution, growth, remodelling, wall shear stress, multi-scale modelling, fluid-solid-growth

## 1. Introduction

Intracranial aneurysms (IAs) are a focal disease of the brain vasculature. They appear as sac-like outpouchings of the arterial wall inflated by the pressure of the blood. The incidence of IAs is surprisingly high: 2%–5% of the adult population are affected. Thankfully, most remain asymptomatic and the risk of rupture is very low: 0.1% to 1% of detected IAs rupture every year [1]. However, rupture leads to fatality in 45% of cases and moderate to severe morbidity for 30% of survivors [2]. Pre-emptive treatment is possible but interventional treatments for unruptured IAs are not without risk and have associated morbidity and mortality rates of <6% and <2.5%, respectively [3]. The increased detection of

*Corresponding author. *E-mail address*: paul.watton@eng.ox.ac.uk.


Selection and/or peer-review under responsibility of the Organizing Committee of The 23rd International Congress of Theoretical and Applied Mechanics, ICTAM2012
doi:10.1016/j.piutam.2014.01.034

unruptured IAs coupled with balancing the potentially fatal scenario of rupture vs. the risk of interventional treatments presents a difficult dilemma for the clinician: to administer treatment, or to monitor the patient?

The exact cause of IAs is unknown, but it is generally accepted that they are a result of a combination of multiple factors, including blood-flow dynamics, arterial wall composition, cell populations, genetics and signalling pathways [4]. Given the lack of understanding of these contributing factors and their complex interplay, modelling may assist in providing fundamental insight into the aetiology of the disease. Moreover, it offers the potential to aid clinical decisions. Current measures for predicting rupture risk are only based on aneurysm size [5]. Consequently, there is a critical need to develop improved patient-specific criteria for rupture to identify the subset of IA patients that would actually benefit from intervention. Biomechanics has an essential role to play in this respect and its application to IA research has grown extensively in the last decade (see, e.g., [6, 7] for a recent review). The focus of this paper is the computational modelling of IA evolution. Such models must quantify the mechanics, the biology and the mechanical environment of the arterial wall. Furthermore, they must account for the interactions between the biology and the mechanics i.e. the mechanobiology of the arterial wall. In this article, we briefly review the requirements of an aneurysm evolution model and present, at this point in time, a state-of-the-art model in the field.

The starting point for a realistic model of aneurysm evolution is a structurally realistic biomechanical model of the healthy artery. Cerebral arteries consist of three layers: the intima, the media, and the adventitia. The intima consists of a monolayer of endothelial cells (ECs) attached to a basement membrane [8]. Whilst ECs contribute little to the mechanical response of the artery, the EC layer has an important function in regulating the effects of haemodynamic forces on the functionality of the arterial wall and acting as a barrier to blood-flow. The media is separated from the intima by the internal elastic lamina and contains a three-dimensional network of elastin fibres and, vascular smooth muscle cells (VSMCs) and collagen fibres which form a fibrous helix with near circumferential orientation [9]. Elastin, a rubber-like, highly extensible protein, gives elasticity to arterial tissue, whilst VSMCs regulate arterial diameter via vasoconstriction and vasodilation [10]. The adventitia is composed predominantly of collagen fibres maintained by fibroblast cells. For the healthy artery, the adventitia acts as a stiff protective sheath to prevent over-distension of the artery, however, during IA evolution, as the medial layer is destroyed, it becomes the predominant load bearing layer and thus its functional role changes.

The structure of the artery is continuously maintained by vascular cells. The functionality of the cells is guided by their local mechanical environment. Cellular responses to forces exerted by the blood-flow are mediated by the extra-cellular matrix (ECM). Indeed, the ECM plays a pivotal role in signalling events that regulate cellular proliferation, migration and apoptosis [11]. The forces are transduced by cellular mechanosensors into a signalling cascade, leading to a host of intra- and inter-cellular responses. For example, ECs respond to increased flow by up-regulating the production of vasodilators. In turn, vasodilators trigger the relaxation of VSMCs to allow the expansion of the arterial wall, and thereby, a return of the wall shear stress (WSS) to baseline levels. Cyclic stretching of the ECM, arising from pulsatile flow, affects the rate of secretion and degradation of ECM material by fibroblasts, i.e., an increase in cyclic strain results in an increase in collagen production and decrease in matrix-degrading enzymes, whilst a decrease in cyclic strain produces the converse result [9]. The dynamic nature of the arterial wall enables it to rapidly respond to altered mechanical conditions, such as altered flow or increased pressure.

Collagen fibres are in a continual state of deposition and degradation with typical half-lives of two months for the healthy artery. In the in vivo configuration, fibres are configured to the ECM in a state of stretch [12]. The continual deposition and degradation of collagen fibres and the observation that they are configured in a state of stretch are essential concepts in mathematical models that simulate arterial growth

and remodelling (G&R) [13–21]. Watton et al. [13] were the first to model aneurysm evolution. Their model utilises a realistic structural model for the arterial wall [9] which is adapted to incorporate variables which define the normalised density (hereon referred to as concentration) of the elastinous and collagenous constituents and the natural reference configurations in which collagen fibres are recruited to bear load. It assumes that collagen fibres are in a continual state of deposition and degradation and that fibres attach to the ECM in a state of stretch, denoted the attachment stretch $\lambda_{\mathrm{AT}}^{\mathrm{C}}$. The implication of these assumptions is that the collagen fabric continuously remodels to maintain its stretch towards a homeostatic value, i.e., $\lambda_{\mathrm{AT}}^{\mathrm{C}}$, in the physiological (loaded) configuration as the aneurysm enlarges. To simulate this, differential equations are employed to evolve the reference configurations in which collagen fibres are recruited to bear load and the collagen concentration adapts to compensate for the loss of load bearing by the elastinous constituents. This approach enables the G&R of the arterial microstructure during aneurysm development to be simulated. Recently, fluid-solid-growth (FSG) models, which couple fluid-solid interactions to the G&R of arterial wall constituents [22] have been developed. Such FSG models have been develop to model IA [7, 23, 24] and abdominal aortic aneurysm [25] evolution.

IA evolution can conceptually be broken down into several stages, namely, inception, enlargement, stablisation and/or rupture. To simulate IA inception, we prescribe a localised loss of elastin in a circular patch of the arterial domain. The collagen fabric adapts to restore homeostasis and a small perturbation to the geometry alters the spatial distribution of haemodynamic stimuli that acts on the endothelial layer of the artery. This enables subsequent degradation of elastin to be linked to deviations of haemodynamic stimuli from homeostatic levels via evolution equations. As the elastin degrades and the collagen fabric adapts (via G&R) an IA evolves. Watton et al. [23] adopted this approach to investigate the evolution of IAs assuming degradation of elastin was linked to high WSS or high WSSG. Given that a region of elevated WSS occurs downstream of the distal neck of the model IA and elevated spatial WSSGs occur in the proximal/distal neck regions, this approach led to IAs that enlarged axially along the arterial domain, i.e. it did not yield IAs with characteristic "berry" topologies. Consequently, Watton et al. [24] linked elastin degradation to low WSS and restricted the degradation of elastin to a localised region of the arterial domain: this yielded IAs of a characteristic saccular shape that enlarged and stabilised in size. Although interesting insights were obtained in both studies, an inherent limitation was that the IAs evolved on a cylindrical section of artery and consequently the spatial distribution of haemodynamic stimuli is non-physiological. This motivated the application of the FSG modelling framework to patient-specific vascular geometries [7]. In this study, a novel, automated algorithmic method is utilised to integrate the model within four patient-specific arterial geometries, which allows the coupling of the G&R of aneurysmal tissue to a physiologically-realistic haemodynamic environment. In the following sections, the computational framework for modelling IA evolution, and the methods to embed the framework within patient-specific arterial geometries are summarised. We illustrate the application of the FSG framework to test the hypothesis that low WSS leads to degradation of the elastinous constituents during IA evolution on four clinical cases and qualitatively compare the predicted evolved IA geometries with those of the clinical cases.

## 2. Methods

### *2.1. Fluid-solid-growth computational framework*

We begin by overviewing the computational framework (illustrated in Fig. 1) that models the fluid and solid mechanics of the arterial wall and explicitly links mechanical stimuli to G&R of the arterial constituents. The computational cycle begins with a quasi-static finite element structural analysis of the aneurysm; whereby the systolic and diastolic equilibrium deformation fields are solved (see [24] for

further details). Stretches and stresses of individual ECM constituents, and the cyclic deformation of vascular cells are obtained from this analysis. The aneurysm geometry is then integrated into a larger geometrical domain to be prepared for computational fluid dynamics analysis. The steady flow is solved, from which hemodynamic quantities of interest (e.g. WSS, WSSG) are obtained. The derived mechanical and hemodynamic quantities are interpolated onto the nodes of the structural mesh, and are fed into G&R algorithms which simulate cell-mediated adaption of tissue; the constitutive model is updated. The cycle then begins again with a structural analysis, solving the equilibrium deformation fields for the updated constitutive model, and, as it continues, the IA develops. The components of the computational framework, i.e. the structural model, haemodynamic modelling and G&R methodology, are discussed in Sects. 2.2, 2.3, and 2.4, respectively.

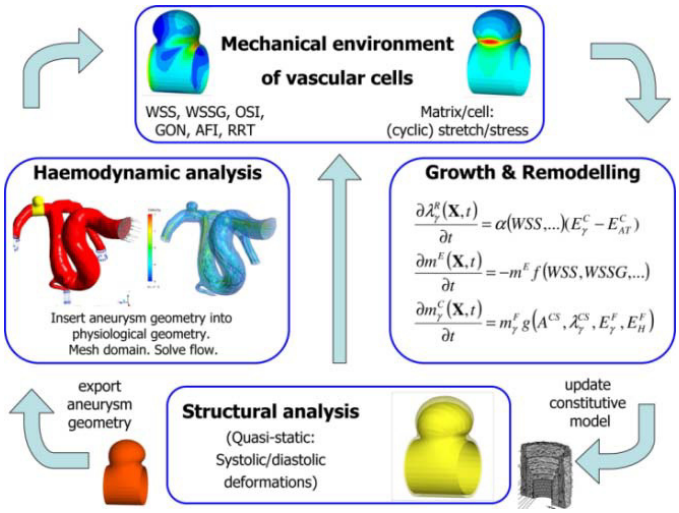


Fig. 1. Fluid-Solid-Growth computational framework

## 2.2. Structural analysis

A geometric nonlinear membrane theory is adopted to model the steady deformation of the arterial wall. The unloaded artery is treated as a thin cylinder of undeformed radius $R$, length $L_1$, and thickness $H$. The thickness of the media $H_M$ is assumed to be 2/3 the thickness of the arterial wall whilst the thickness of the adventitia $H_A$=$H$/3. A body-fitted coordinate system is used to describe the cylindrical membrane with axial and azimuthal Lagrangian coordinates $\theta_1 \in [0, L]$ and $\theta_2 \in [0, 2\pi R]$, respectively. The artery is subject to a physiological axial pre-stretch $\lambda_z$ and at a systolic pressure $p$ it has a circumferential stretch of $\lambda_0$. Formation and development of the aneurysm is assumed to be a consequence of G&R of the material constituents of the artery; the distal and proximal ends of the arterial domain are considered fixed as the aneurysm enlarges. The principal of stationary potential energy is the governing equation for the steady deformation of the arterial wall. It requires that the first variation of the total potential energy vanishes, i.e.

$$\delta\Pi_{\text{int}} - \delta\Pi_{\text{ext}} = 0, \tag{1}$$

where $\delta\Pi_{\text{int}}$ represents the variation of the internal potential energy stored in the arterial wall, whilst $\delta\Pi_{\text{ext}}$ is the variation of the external potential energy due to the traction that acts on the arterial wall.

Appropriate functional forms for the spatially and temporally heterogeneous strain-energy functions (SEFs) for the media $\Psi_{\mathrm{M}}$ and adventitia $\Psi_{\mathrm{A}}$ must be specified so that $\delta\Pi_{\mathrm{int}}$ can be computed. Details of the theoretical formulation to describe the deformation of the arterial wall and the numerical formulation to solve Eq. (1) can be found in [14].

The arterial wall is modelled as two layers. The inner layer models the mechanical response of the media (and intima), with contributions from the elastinous constituents (ground substance, elastin fibres and passive VSMCs) and a double-helical pitch of collagen fibres with orientations $\gamma_{\mathrm{M}_p}$ to the azimuthal axis: $p=\pm$ denote positively ($\gamma_{\mathrm{M}+}>0$) and negatively ($\gamma_{\mathrm{M}+}<0$) wound fibres, respectively. The outer layer models the mechanical response of the adventitia, which is considered to have a small elastinous contribution and a double-helical pitch of collagen fibres with orientations $\gamma_{\mathrm{A}_p}$ ($p=\pm$) to the azimuthal axis. The mechanical response of each layer is modelled as the sum of a neo-Hookean SEF [26] and a highly nonlinear SEF which represents the mechanical response of the collagen. Watton et al. [13] sophisticated the HGO constitutive model [8] to incorporate: (1) constituent concentration variables which define the ratio of the mass density of a constituent at time $t$ to the mass density at time $t$=0 and enable the growth/atrophy of constituents to be simulated; (2) recruitment stretch variables, which define a mapping between the unloaded reference configuration and reference configuration in which the collagen fibres begin to be recruited to load bearing. Fields of spatially and temporally dependent fibre recruitment stretch $\lambda^{\mathrm{R}}_{J_p}(\theta_1,\theta_2,t)$ and concentration $m^{\mathrm{C}}_{J_p}(\theta_1,\theta_2,t)$ variables are defined for the media and adventitia throughout the arterial wall; $J$=M, A denotes the media (M) and the adventitia a. The SEFs for the elastinous contributions in the medial and adventitia are multiplied by a normalised spatially and temporally dependent concentration function, denoted $m^{\mathrm{E}}(\theta_1,\theta_2,t)$. This is employed to prescribe the degradation of the elastinous constituents, where $m^{\mathrm{E}}(\theta_1,\theta_2,t=0)=1$. The SEFs are

$$\Psi_J = m^{\mathrm{E}} K^{\mathrm{E}}_J (E_{11}+E_{22}+E_{33}) + \Sigma_{P=\pm,E^{\mathrm{C}}_{J_p}} m^{\mathrm{C}}_{J_p} K^{\mathrm{E}}_J \{[A^{\mathrm{C}}(E^{\mathrm{C}}_{J_p})^2]-1\}, \qquad J=\mathrm{M},\mathrm{A}. \tag{2}$$

The Green–Lagrange (GL) strains of the elastin, i.e. $E_{11}, E_{22}$, and $E_{33}$ are defined relative to the unloaded configuration; in the initial cylindrical configuration, these represent strains in the axial, azimuthal and radial directions, respectively. The GL strains for the collagen fibres are denoted by $E^{\mathrm{C}}_{J_p}(\theta_1,\theta_2,t)$ and are defined relative to the configuration in which the collagen fibres are recruited to load bearing. More specifically, the GL strains $E^{\mathrm{C}}_{J_p}$ of the collagen fibres are a function of the GL strains of the elastin resolved in the directions of the collagen fibres, denoted $E^{\mathrm{C}}_{J_p}$, where

$$E^{\mathrm{C}}_{J_p} = \frac{E_{J_p} - E^{\mathrm{R}}_{J_p}}{1+2E^{\mathrm{R}}_{J_p}}, \tag{3}$$

$E^{\mathrm{R}}_{J_p} = ((\lambda^{\mathrm{R}}_{J_p})^2-1)/2$, and $E_{J_p} = E_{11}\sin^2\gamma_{J_p} + E_{22}\cos^2\gamma_{J_p} + E_{12}\sin\gamma_{J_p}\cos\gamma_{J_p}$.

The material parameters for the elastinous constituent are denoted by $K^{\mathrm{E}}_J$ whilst $K^{\mathrm{C}}_J$ and $A^{\mathrm{C}}$ are parameters that relate to the collagen fabric. In the systolic configuration, the artery has a radius $r_S$, an axial pre-stretch of 1.3, and a circumferential stretch of 1.25. It is assumed that 80% of the load is borne by the elastinous constituents. The magnitude of the collagen attachment stretch $\lambda^{\mathrm{C}}_{\mathrm{AT}}$ is defined to be the stretch in the collagen fabric at systole at $t=0$. It is assumed that the elastinous response of the adventitia

is an order of magnitude weaker than that of the media, i.e. $K_A^E = K_M^E/10$ where the ratio of the medial and adventitial collagen material parameters is $K_A^E = K_M^C/4$. The three independent material parameters $K_A^E$, $K_M^C$ and $A^C$ are determined so that the SEFs adequately model the mechanical behaviour of the artery [19]. The main geometrical and physiological parameters for the examples presented in this paper are summarised in Table 1 below:

Table 1. Parameters for the four internal carotid cases

| **Radii** | **Symbol** | **Case 1** | **Case 2** | **Case 3** | **Case 4** |
|---|---|---|---|---|---|
| Reference configuration | $R$ (mm) | 2.011 | 1.785 | 1.741 | 1.813 |
| At systole | $r_s$ (mm) | 2.900 | 3.570 | 2.612 | 2.719 |
| **Wall thickness** | | | | | |
| Total | $H$ (mm) | 0.402 | 0.357 | 0.348 | 0.363 |
| Media | $H_M$ | 0.268 | 0.238 | 0.232 | 0.242 |
| Adventitia | $H_A$ | 0.134 | 0.119 | 0.116 | 0.121 |

| **Fibre orientation** | **Symbol** | |
|---|---|---|
| Media | $\gamma_{M+}, \gamma_{M-}$ (°) | $+30°, -30°$ |
| Adventitia | $\gamma_{A+}, \gamma_{A-}$ | $+60°, -60°$ |
| **Applied pressure, kinematics** | | |
| Systolic pressure | $p$ (kPa) | 16 |
| Axial pre-stretch | $\lambda_z$ | 1.3 |
| Ratio of systolic to diastolic circumferential diameters | $\lambda_\Theta^s$ | 1.1 |
| **Attachment stretch** | $\lambda_{AT}^C$ | 1.07 |
| **Recruitment stretches (t=0)** | | |
| Media | $\lambda_{M+}^R, \lambda_{M-}^R$ | 1.18 |
| Adventitia | $\lambda_{A+}^R, \lambda_{A-}^R$ | 1.20 |

### *2.3. Computational fluid dynamics methodology*

To achieve physiologically realistic flow in the region where the IA develops, extensions are attached to the structural model of the artery/aneurysm using vasculature geometry obtained from clinical imaging data. The process of connecting the structural model of the healthy artery (which is initially cylindrical) to the physiological vasculature is illustrated in Fig. 2. Based on the diameters and distance between the physiological boundaries, a cylinder is generated to fit between the up- and downstream physiological surfaces (Fig. 2a). The physiological boundaries are re-interpolated such that each comprises 120 equidistant points (Fig. 2b(i)). Corresponding physiological and cylinder boundary points are determined by finding the point on the physiological boundary that is at the shortest distance from a specified point on the cylinder boundary; all other points are then paired in anti-clockwise order (Fig. 2b(ii)). A series of interpolating splines (using sigmoidal functions), normal to each boundary, are generated (shown as a series of points in Fig. 2c(i)). These are connected to form a triangulated surfaces (Fig. 2c(ii)) which connects the cylindrical section smoothly to the upstream and downstream sections of physiological arterial geometry.

The methodological approach to solve the haemodynamics as the aneurysm evolves proceeds as follows. The geometry of the aneurysmal section is exported from the structural solver to the meshing suite ANSYS ICEM (ANSYS Inc, Canonsburg, PA). ANSYS ICEM automatically integrates the aneurysmal section into the physiological domain and generates an unstructured tetrahedral mesh with prism layers

lining the boundary in a scripted-automated manner for the fluid domain. After meshing, appropriate boundary conditions are applied and the flow is solved by ANSYS CFX (ANSYS Inc, Canonsburg, PA) which solves the incompressible Navier–Stokes equations using a finite volume formulation [27]. The solver is based on a coupled approach (i.e., velocities and pressure are cast and solved as a single system) and a fully implicit time discretisation, where needed. Blood is modelled as a Newtonian fluid with constant density $\rho = 1\,069$ kg·m$^{-3}$ and constant viscosity $\mu = 0.003\,5$ Pa·s. At the arterial wall, a no slip condition is applied for a rigid wall. Whilst a pulsatile flow analysis is necessary to explore more sophisticated G&R hypotheses, for the FSG model presented in this paper, we adopt a steady flow analysis to reduce the computational cost of the simulations. The similarity of the spatial WSS/WSSG distributions for steady and pulsatile flow simulations [24] suggests that adopting steady flow may be a reasonable approach for the purposes of investigating phenomenological hypotheses that explore the link between G&R of aneurysmal tissue and deviations of the WSS/WSSG from normotensive values. Boundary conditions are taken from a 1D circulation model [28] incorporated within @neufuse software, a software suite developed as part of the @neurIST EU project.

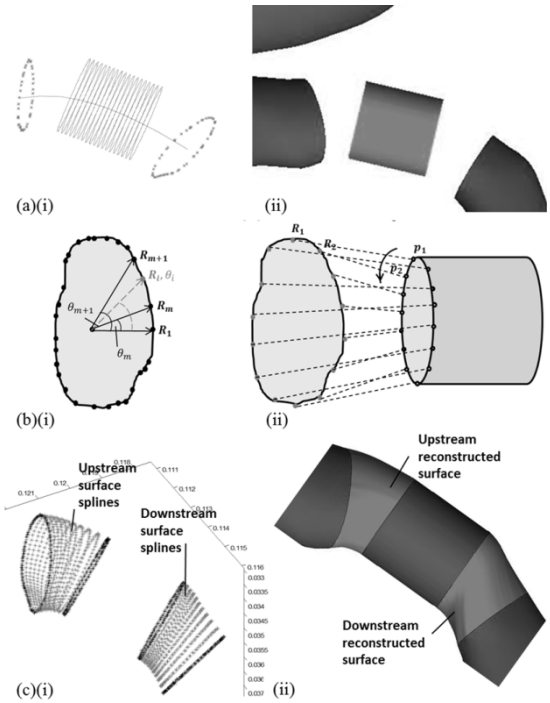


Fig. 2. Surface reconstruction algorithm. (a)(i) & (ii) cylinder generation and positioning between physiological boundaries; (b)(i) & (ii) physiological boundary re-interpolation to achieve equidistant boundary points; (c)(i) & (ii) generation of splines, connected to form triangulated surfaces.

## *2.4. Growth and remodelling*

### *2.4.1. Degradation of elastinous constituents*

Histologically, a saccular IA is characterised by an abrupt loss of the medial layer at the IA neck and a thin collagenous tissue within the IA dome [29]. To capture the loss of the medial layer, first an initial

degradation is prescribed to occur within a small circular patch of the arterial domain (for details, see [23]), which results in a small outpouching in the arterial wall. This outpouching results in a disturbance to the local hemodynamic environment, and, in turn, a change in the local WSS from normotensive levels. Subsequent degradation is then linked to locally low values of WSS

$$\frac{\partial m^{\mathrm{E}}}{\partial t} = -F_{\mathrm{D}}(\tau(\theta_1,\theta_2,t))D_{\max}m^{\mathrm{E}}(\theta_1,\theta_2,t), \tag{4}$$

where $F_{\mathrm{D}}$ is a spatially-dependent function of WSS (denoted by $\tau$)

$$F_{\mathrm{D}}(\tau(\theta_1,\theta_2,t)) = \begin{cases} 0, & \tau(\theta_1,\theta_2,t) \geq \tau_{\mathrm{crit}}. \\ \left(\dfrac{\tau_{\mathrm{crit}} - \tau(\theta_1,\theta_2,t)}{\tau_{\mathrm{crit}} - \tau_X}\right), & \tau_X < \tau(\theta_1,\theta_2,t) < \tau_{\mathrm{crit}}. \\ 1, & \tau(\theta_1,\theta_2,t) \leq \tau_{\mathrm{crit}}. \end{cases} \tag{5}$$

We suppose that for WSS magnitudes above a critical value, $\tau_{\mathrm{crit}}$, no degradation occurs ($F_{\mathrm{D}}=0$) whereas if the WSS is equal to or below a critical minimum value, denoted $\tau_X$ then the maximum rate of degradation occurs ($F_{\mathrm{D}}=1$). For values between $\tau_X$ and $\tau_{\mathrm{crit}}$, the degradation function $F_{\mathrm{D}}$ is assumed, for simplicity, to have a quadratic form. Given that the spatial distribution of WSS varies between geometries, the values of $\tau_{\mathrm{crit}}$ and $\tau_X$ need to be specified for each case (Table 2). Let $\tau_1$ and $\tau_2$ denote the minimum values of WSS within the circular patch for the conceptual healthy artery and the artery following the prescribed inception, respectively. On the assumption that the perturbation to the geometry leads to a local decrease in WSS, i.e. $\tau_2<\tau_1$, we take $\tau_{\mathrm{crit}}=\tau_1$ and $\tau_X=\tau_2$.

Table 2: Critical WSS thresholds for onset of elastin degradation and maximum elastin degradation

| Critical WSS thresholds | Symbol | Case 1 | Case 2 | Case 3 | Case 4 |
|---|---|---|---|---|---|
| Elastin degradation | $\tau_{\mathrm{crit}}$ (Pa) | 9.2 | 7 | 6.6 | 4.7 |
| Maximum elastin degradation | $\tau_X$ (Pa) | 4.59 | 3.7 | 4.4 | 3.9 |

### *2.4.2. Collagen remodelling*

Collagen fibres are in a continual state of deposition and degradation and attach to the artery in a state of stretch. Watton et al. [13] hypothesised that the collagen fibres are configured to achieve a maximum stretch during the cardiac cycle and introduced the terminology attachment stretch $\lambda_{\mathrm{AT}}^{\mathrm{C}}$. The magnitude of the recruitment stretch variables $\lambda_{J_p}^{\mathrm{R}}(\theta_1,\theta_2,t)$ are defined such that at $t=0$, the collagen stretches are equal to the attachment stretch throughout the domain (see [18] for details). As the geometry evolves, the recruitment stretches evolve so that the maximum GL strain of the collagen during the cardiac cycle remodels towards the attachment strain, denoted $E_{\mathrm{AT}}^{\mathrm{C}}$. Initially, it was assumed that maximum strains are achieved in the systolic configuration and thus the remodelling scheme was implemented computationally by considering the steady deformation of the arterial at systolic pressure [13]. However, as the geometry becomes more complex this is not necessarily true [13]. Consequently, the methodology has recently been updated (see [25]) to assume that the maximum strains occur in either the systolic or diastolic configuration, i.e.

$$\frac{\mathrm{d}\lambda_{J_p}^R}{\mathrm{d}t} = \alpha \frac{E_{J_p}^{\mathrm{C}}\Big|_{\max} - E_{\mathrm{AT}}^{\mathrm{C}}}{E_{\mathrm{AT}}^{\mathrm{C}}}, \tag{6}$$

where $E_{\mathrm{AT}}^{\mathrm{C}} = ((\lambda_{\mathrm{AT}}^{\mathrm{C}})^2 - 1)/2$ and $E_{J_p}^{\mathrm{C}}\Big|_{\max} = \max\left( E_{J_p}^{\mathrm{C}}\Big|_{\mathrm{sys}} - E_{J_p}^{\mathrm{C}}\Big|_{\mathrm{dias}} \right)$. $E_{J_p}^{\mathrm{C}}\Big|_{\mathrm{sys}}$ and $E_{J_p}^{\mathrm{C}}\Big|_{\mathrm{dias}}$ are the magnitudes of the collagen strains evaluated in the systolic and diastolic configurations, respectively. For the analysis in this paper, $\alpha = 0.6^{-1}$ years.

*2.4.3. Collagen growth*

In vascular homeostasis, the mass of the collagenous constituents is constant even though the fibers are in a continual state of deposition and degradation. However, in response to perturbations to the mechanical environment, vascular cells can respond by up (down)-regulating synthesis and down (up)-regulating degradation leading to a net increase (decrease) in mass. We outline the algorithm proposed to simulate this [18, 25]. The key assumptions of which are

(1) The reference configuration of the cells is equal to the reference configuration of the constituents that they are maintaining;
(2) The number of cells is proportional to the mass of constituents they are maintaining;
(3) In vascular homeostasis, the mass of the constituents is constant.

From these assumptions, the simplest (linear) equation for adapting the normalized mass-density of the collagenous constituents can be derived to be

$$\frac{\mathrm{d}m_{J_p}^{\mathrm{C}}}{\mathrm{d}t} = m_{J_p}^{\mathrm{C}} \beta \frac{E_{J_p}^{\mathrm{C}}\Big|_{\max} - E_{\mathrm{AT}}^{\mathrm{C}}}{E_{\mathrm{AT}}^{\mathrm{C}}}, \tag{7}$$

where $\beta$ is a phenomenological growth parameter. Note that this equation is derived by considering perturbations of the strains of the vascular cells from homeostatic levels. It is the assumption that the reference configuration of the cells is equal to that of the constituent that they are maintaining leads to it being expressed as a function of the strains of the collagen fibers. To simplify the presentation of the results, an average concentration of the medial and adventitial collagen fibres is defined as

$$m^{\mathrm{C}} = \frac{1}{H}\left( H_{\mathrm{M}} \frac{m_{\mathrm{M+}}^{\mathrm{C}} - m_{\mathrm{M-}}^{\mathrm{C}}}{2} + H_{\mathrm{A}} \frac{m_{\mathrm{A+}}^{\mathrm{C}} - m_{\mathrm{A-}}^{\mathrm{C}}}{2} \right). \tag{8}$$

## 3. Results

Figure 3 illustrates four examples of IAs evolving on physiological sections of vasculature: (a) the clinical geometry with patient IA; (b) the vasculature with the IA removed and replaced by a cylindrical section to represent a section of healthy artery; (c) an evolved IA. Figures 3b and 3c show the WSS distributions for the four cases at $t = 0$ and $t = 10$ years, respectively. It can be seen that for cases 1 and 2, the IA geometries grew larger, and evolved more symmetrically compared to the evolved IA geometries for cases 3 and 4. The difference in size and asymmetry are accounted for by the differences in the WSS spatial distribution. Cases 1 and 2 exhibit evolving patches of low WSS at both the proximal and distal regions of the IA dome. This drives elastin degradation in these locations and results in a more symmetric aneurysmal geometry. For cases 3 and 4, a very small patch of low WSS is localised at the proximal part of the geometry. Consequently, the IA evolves asymmetrically towards the proximal part of the artery and stabilizes.

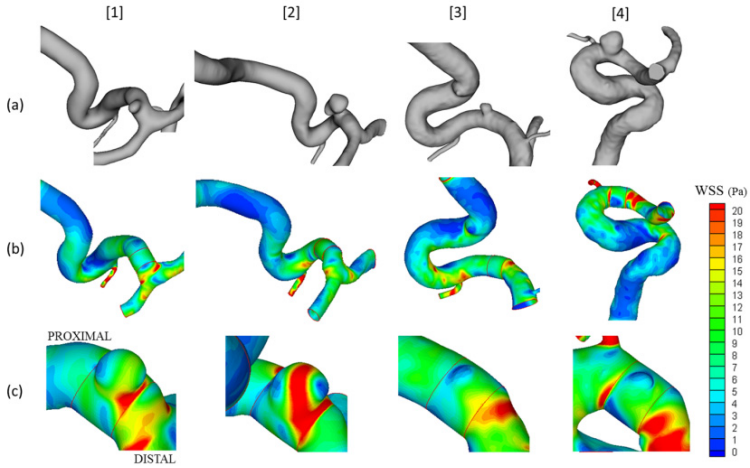


Fig. 3. (a) 4 patient-specific aneurysm geometries; (b) the IA is virtually removed and replaced with a cylindrical section to represent a section of healthy artery at $t = 0$; (c) WSS of the simulated IA at $t = 11$ years. The colourmaps depict the WSS distribution.

Figure 4 examines in more detail the evolution of the IA depicted in case 2 and illustrates the evolving: (a) elastin concentration; (b), (c) elastin strains; (d) medial collagen strain; (e) average collagen concentration; (f) cyclic areal stretch (ratio of areal stretch at systole to areal stretch at diastole). Elastin is observed to degrade most rapidly in localised regions of the distal and proximal dome corresponding to the regions of locally low WSS (see Fig. 3c, case 2). Note that whilst there is significant enlargement of the geometry, the collagen strains increase negligibly; this is due to the remodelling of the natural reference configuration in which the fibres are recruited to load bearing. In response to the increase in collagen strain the evolution equation for the mass of collagen acts to increase the collagen concentration to compensate for the loss of load bearing by the elastinous constituents. The cyclic areal stretch $A^{CS}$ remains high in the lateral part of the dome, but is observed to reduce at the top, distal and proximal parts of the dome. It increases to a maximum of 2.7. Tthis seems unrealistically high, i.e. it is unlikely cells could remain attached to the tissue when subject to such large deformation during the cardiac cycle. This suggests the need to couple the evolving collagen concentration to the magnitude of the cyclic areal stretch. In fact, this has been integrated into the G&R methodology and has been found to bean effective method to maintain the magnitude of $A^{CS}$ to within a physiologically realistic range [7, 25].

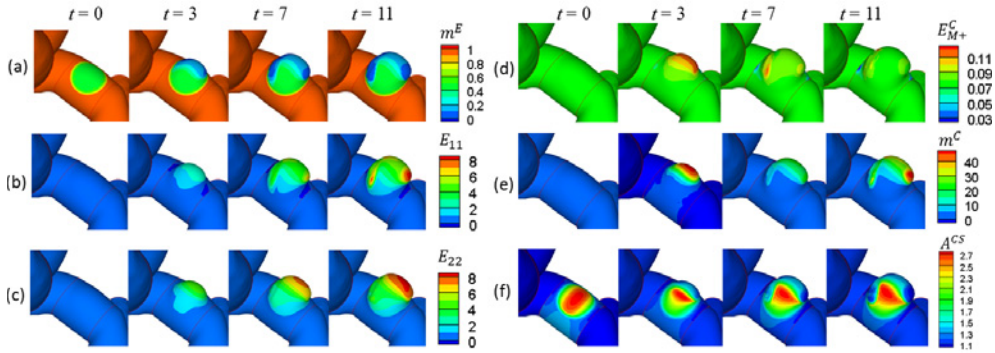


Fig. 4. Evolution of the (a) elastin concentration, (b) axial and (c) azimuthal elastin GL strains, (d) medial collagen strain (e) average collagen concentration and (f) cyclic areal stretch for case 2 at $t = 0$, 3, 7 and 11 years.

## 3. Discussion

We presented a novel FSG framework for modelling IA evolution on physiological geometries. The framework incorporates a realistic structural model of the arterial wall and it couples G&R to cyclic deformation and to the local haemodynamic stimuli that act on ECs. To simulate IA inception, elastin degradation is prescribed to occur within a small circular patch of the cylindrical domain to generate an initial perturbation to the geometry; subsequent degradation is then linked to low WSS. The remodelling of collagen fibres is simulated by evolving the collagen recruitment stretches, to capture the effect of new fibres being configured to achieve a peak stretch of $\lambda_{\mathrm{AT}}^{\mathrm{C}}$ during the cardiac cycle. Growth of collagen is simulated by evolving the fibre concentration. Interestingly, the direction of enlargement of the evolving model IA domes of cases 2, 3 and 4 appears to (qualitatively) reflect the corresponding original IA geometry of each case (see Fig. 5).

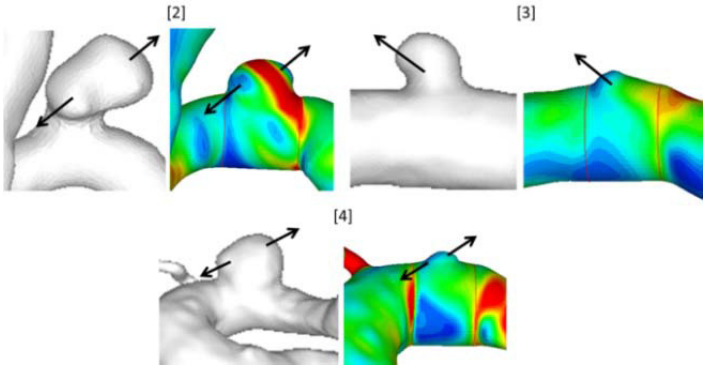


Fig. 5. Similarities in the direction of enlargement of the model IA geometries of cases 2, 3 and 4 to their physiological counterparts

The results of this study appear to give some support to the commonly stated hypothesis that low WSS is a driver of IA evolution. For instance, Tanoue et al. [43] performed CFD simulations on silicon models of 2 patient-specific cases (one growing, one non-growing) and compared the haemodynamic patterns over 4 stages of enlargement. In the case of the enlarging IA, they found an elevated WSS away from the region of enlargement, high WSSG in the region adjacent to enlargement, and low WSS in the region of enlargement. Interestingly, they did not observe low WSS in the dome of the non-growing aneurysm. In similar studies, both Jou et al. [33] and Boussel et al. [34] found a positive correlation between low WSS and regions of greatest growth of the aneurysm dome. A commonly-proposed mechanism for low-WSS-induced destructive remodelling is via the release of matrix metallo-proteinases (MMPs) by inflammatory cells. Aoki and Nishimura [35] recently characterised the shear-stress sensitive transcriptional factor NF-κB as a mediator of chronic inflammation in aneurysmal walls by induction of the MCP-1 pathway. Kanematsu et al. [36] induced aneurysms on adult mice, and found that those with a suppressed MCP-1 pathway had a reduced monocyte/macrophage count, impaired macrophage function, and in general showed a lower incidence of aneurysm formation.

However, it may be that that disturbed flow arising in low WSS conditions may be the real cause of destructive remodelling. Tremmel et al. [37] performed numerical studies in which the aneurysm-to-parent artery size ratio was virtually varied, and observed that aneurysm enlargement is followed by a decreased WSS and increased flow instability, including high wall shear stress gradients. In disturbed flow conditions, ECs experience oxidative stress, and increased expression of inflammatory markers and monocyte recruitment [38]. When subjected to disturbed flow, ECs show no preferential alignment and

exhibit a polygonal shape [39, 40]. This may lead to a widening of cellular junctions, and thereby facilitate monocyte migration into the arterial wall. Indeed, ex-vivo study on ECs in porcine iliac arteries [41] showed that transendothelial permeability is more likely to be elevated in low WSS conditions, and particularly so, in the presence of a high WSSG.

Hence, although the results of this study suggest support for the hypothesis that growth is driven by low WSS, it is possible that in reality the nature of the intra-aneurysmal flow—and not the magnitude of WSS—is the critical factor for IA growth. The four physiological cases presented here comprise a small study, and thus the results and conclusions must be interpreted with caution. Several indices associated with oscillatory shear arising from flow pulsatility have also been proposed in an attempt to determine arterial regions most susceptible to IA formation [6]. Furthermore, whilst models of aneurysm evolution have gained increasing sophistication over the past decade, undoubtedly, many further improvements are required. For instance, there is a need to incorporate explicit representations of vascular cells (ECs, VSMCs and fibroblasts), their interactions and the signalling networks [42] that link the stimuli acting on them to their functionality in physiological and pathological conditions. This will better inform hypotheses for haemodynamics-dependent G&R.

There is also a need for implementation of more sophisticated constitutive models to represent, e.g. the collagen fibre recruitment distribution [43, 44] and dispersion, and the active and passive response of VSMCs [45]. Lastly, improved understanding and modelling of how this complex micro-structure adapts in pathological conditions is needed: the modelling framework needs to be validated and/or calibrated against physiological data; animal models undoubtedly have a role to play in this respect [46]. This motivates the need for multi-scaled models which integrate the biology and the (solid and fluid) biomechanics of the arterial wall, i.e. FSG models, such as the one we have presented here. Such models provide the foundations to model not only aneurysm evolution, but other vascular diseases and may ultimately lead to predictive models that have diagnostic application on a patient specific basis. Of course, the challenging and multi-disciplinary nature of such research implies that to be successful in this field, collaborative research is essential.

## Acknowledgements

Alisa Selimovic is a doctoral student funded by the Robert Menzies Memorial Trust. Paul Watton is a University Research Lecturer in the Institute of Biomedical Engineering and is funded by The Centre of Excellence in Personalized Healthcare (funded by the Wellcome Trust and EPSRC, WT 088877/Z/09/Z). This support is gratefully acknowledged.

## References

[1] Juvela S. Treatment options of unruptured intracranial aneurysms. *Stroke* 2004; **35**: 372–374.

[2] Brisman JL, Song JK, Newell DW. Cerebral aneurysms. *The New England journal of medicine* 2006; **355**: 928–939.

[3] Peters DG, Kassam AB, Feingold E, Heidrich-O'Hare E, Yonas H, Ferrell RE, et al. molecular anatomy of an intracranial aneurysm: Coordinated expression of genes involved in wound healing and tissue remodeling. *Stroke* 2001; **32**: 1036–1042

[4] Robertson AM, Watton PN. Computational fluid dynamics in aneurysm research: critical reflections, future directions. *AJNR* 2012; **33**: 992–995.

[5] Ventikos Y, Bowkera TJ, Wattona PN, Kakalisa NMP, Byrneb JV. Risk evaluation and interventional planning for cerebral aneurysms: computational models for growth, coiling and thrombosis. *International Journal of Computational Fluid Dynamic* 2009; **23**: 595–607.

[6] Sforza DM, Putman CM, Cebral JR. Computational fluid dynamics in brain aneurysms. *International Journal for Numerical Methods in Biomedical Engineering* 2011; **28**: 801–808.

[7] Watton PN, Ventikos Y, Holzapfel GA. Modelling Cerebral Aneurysm Evolution. In: McGloughlin T, editors. *Biomechanics*

*and mechanobiology of aneurysms*, Heidelberg: Springer-Verlag; 2011; 307–322

[8] Robertson AM, Watton PN. Mechanobiology of the Arterial Wall. In: Kuznetsov A, Becker S, editors. *Transport in biological media,* Elsevier; 2013.

[9] Holzapfel GA, Gasser TC, Ogden RW. A new constitutive framework for arterial wall mechanics and a comparative study of material models. *Journal of Elasticity* 2000; **61**: 1–48.

[10] Wang JH-C, Thampatty BP. An introductory review of cell mechanobiology. *Biomech Model Mech* 2006; **5**: 1–16.

[11] Cummins PM, von Offenberg Sweeney N, Killeen MT, Birney YA, Redmond EM, Cahill PA. Cyclic strain-mediated matrix metalloproteinase regulation within the vascular endothelium: a force to be reckoned with. *American Journal of Physiology. Heart and Circulatory Physiology* 2007; **292**: H28–42.

[12] Alberts B, Johnson A, Lewis J, Raff M, Roberts K, Walter P. *Molecular biology of the cell.* 4th ed. New York: Garland Science; 2002.

[13] Watton PN, Hill NA, Heil M. A mathematical model for the growth of the abdominal aortic aneurysm. *Biomechanics and Modeling in Mechanobiology* 2004; **3**: 98–113.

[14] Gleason RL, Taber LA, Humphrey JD. A 2-D model of flow-induced alterations in the geometry, structure, and properties of carotid arteries. *Journal of Biomechanical Engineering* 2004; **126**: 371–381.

[15] Baek S, Rajagopal KR, Humphrey JD. A Theoretical model of enlarging intracranial fusiform aneurysms. *Journal of Biomechanical Engineering* 2006; **128**: 142–149

[16] Kroon M, Holzapfel GA. Modeling of saccular aneurysm growth in a human middle cerebral artery. *Journal of Biomechanical Engineering* 2008; **130**: 051012.

[17] Watton PN, Ventikos Y. Modelling the growth and stabilisation of cerebral aneurysms. *Math Med Biol* 2009; **26**: 133–164.

[18] Watton PN, Ventikos Y. Modelling evolution of saccular cerebral aneurysms. *J Strain Analysis* 2009; **44**: 375–389.

[19] Watton PN, Hill NA. Evolving mechanical properties of a model of abdominal aortic aneurysm. *Biomechanics and Modeling in Mechanobiology* 2009; **8**: 25-42.

[20] Schmid H, Watton PN, Maurer MM, Wimmer J, Winkler P, Wang YK. Impact of transmural heterogeneities on arterial adaptation: application to aneurysm formation. *Biomechanics and Modeling in Mechanobiology* 2010; **9**: 295–315.

[21] Schmid H, Grytsan A, Poshtan E, Watton PN, Itskov M. Influence of differing material properties in media and adventitia on arterial adaptation - application to aneurysm formation and rupture. *Computer methods in biomechanics and biomedical engineering* 2013; **16**: 33–53.

[22] Humphrey JD, Taylor CA. Intracranial and abdominal aortic aneurysms: similarities, differences, and need for a new class of computational models. *Annual Review of Biomedical Engineering* 2008; **10**: 221–246.

[23] Watton PN, Raberger NB, Holzapfel GA, Ventikos Y. Coupling the haemodynamic environment to the evolution of cerebral aneurysms: computational framework and numerical examples, *ASME Journal of Biomedical Engineering* 2009; **131**: 101003.

[24] Watton PN, Selimovic A, Raberger NB, Huang P, Holzapfel GA,Ventikos Y. Modelling Evolution and the evolving mechanical environment of saccular cerebral aneurysms. *Biomechanics and Modeling in Mechanobiology* 2011; **10**: 109–132

[25] Watton PN, Huang H, Ventikos Y. Multi-scale modelling of vascular disease: Abdominal aortic aneurysm evolution. In: Geris L, editor. *Computational modeling in tissue engineering. series: Studies in mechanobiology, tissue engineering and biomaterial*. Heidelberg: Springer Berlin/Heidelberg; 2012, 309–341.

[26] Watton PN, Ventikos Y, Holzapfel GA. Modelling the mechanical response of elastin for arterial tissue. *J Biomechanics* 2009; **42**: 1320–1325.

[27] Ferziger JH, Peric M. *Computational Methods for Fluid Dynamics.* 3rd ed. Heidelberg: Springer-Verlag; 2002.

[28] Reymond P, Merenda F, Perren F, Rüfenacht D, Stergiopulos N. Validation of a one-dimensional model of the systemic arterial tree. *American journal of physiology. Heart and circulatory physiology* 2009; **297**: H208– H222.

[29] Kondo S, Hashimoto N, Kikuchi H, Hazama F, Nagata I, Kataoka H. Cerebral aneurysms arising at nonbranching sites. an experimental study. *Stroke* 1997; **28**: 398–404.

[30] Howard AB, Alexander RW, Nerem RM, Griendling KK, Taylor WR. Cyclic strain induces an oxidative stress in endothelial cells. *AJNR* 1997; **272**: C421– C427.

[31] Iba T, Sumpio BE. Morphological response of human endothelial cells subjected to cyclic strain in vitro. *Microvascular*

*Research* 1991; **42**: 245–254.

[32] Tanoue T, Tateshima S, Villablanca JP, Viñuela F, Tanishita K. Wall shear stress distribution inside growing cerebral aneurysm. *AJNR* 2011; **32**: 1732–1737.

[33] Jou LD, Wong G, Dispensa B, Lawton MT, Higashida RT, Young WL, et al. Correlation between lumenal geometry changes and hemodynamics in fusiform intracranial aneurysms. *AJNR* 2005; **26**: 2357–2363.

[34] Boussel L, Rayz V, McCulloch C, Martin A, Acevedo-Bolton G, Lawton M, et al., Aneurysm growth occurs at region of low wall shear stress: patient-specific correlation of hemodynamics and growth in a longitudinal study. *Stroke* 2008; **39**: 2997–3002.

[35] Aoki T, Nishimura M. Molecular mechanism of cerebral aneurysm formation focusing on NF-κB as a key mediator of inflammation. *Journal of Biorheology* 2010; **24**: 16–21 .

[36] Kanematsu Y, Kanematsu M, Kurihara C, Tada Y, Tsou TL, van Rooijen N, et al. Critical roles of macrophages in the formation of intracranial aneurysm. *Stroke* 2011; **42**: 173–178.

[37] Tremmel M, Dhar S, Levy EI, Mocco J, Meng H. Influence of intracranial aneurysm-to-parent vessel size ratio on hemodynamics and implication for rupture: results from a virtual experimental study. *Neurosurgery* 2009; **64**: 622–630.

[38] Shyu K. Mechanosensitivity and Mechanotransduction. In: A. Kamkin, I. Kiseleva, editors. *Stress: The International Journal on the Biology of Stress* 2011; 193–217.

[39] Chien S. Mechanotransduction and endothelial cell homeostasis: the wisdom of the cell. *American journal of physiology. Heart and circulatory physiology* 2007; **292**: H1209– 1224.

[40] Chien S. Effects of disturbed flow on endothelial cells. *Annals of Biomedical Engineering* 2008; **36**: 554–562.

[41] LaMack JA, Friedman MH. Individual and combined effects of shear stress magnitude and spatial gradient on endothelial cell gene expression. *American Journal of Physiology. Heart and Circulatory Physiology* 2007; **293**: H2853–2859.

[42] Ho H, Suresh V, Kang W, Cooling MT, Watton PN, Hunter PJ. Multiscale modeling of intracranial aneurysms: cell signaling, hemodynamics, and remodeling. *IEEE Transactions on Biomedical Engineering* 2011; **58**: 2974–2977.

[43] Hashimoto T, Meng H, Young WL. Intracranial aneurysms: links among inflammation, hemodynamics and vascular remodeling. *Neurological research* 2006; **28**: 372–380.

[44] Hill MR, Duan X, Gibson GA, Watkins S, Robertson AM. A theoretical and non-destructive experimental approach for direct inclusion of measured collagen orientation and recruitment into mechanical models of the artery wall. *J of Biomechanics* 2012; **45**: 762–771.

[45] Hill MA, Meininger GA. Arteriolar vascular smooth muscle cells: Mechanotransducers in a complex environment. *The international journal of biochemistry & cell biology* 2012; **44**: 1505–1510.

[46] Zeng Z, Kallmes DF, Durka MJ, Ding Y, Lewis D, Kadirvel R, Robertson AM. Hemodynamics and anatomy of elastase-induced rabbit aneurysm models: similarity to human cerebral aneurysms? *AJNR* 2011; **32**: 595–601.